ELSEVIER

Organic Electronics 3 (2002) 33–42

Organic Electronics

www.elsevier.com/locate/orgel

Current noise spectroscopy on mLPPP based organic light emitting diodes

G. Ferrari [a], D. Natali [a], M. Sampietro [a,*], F.P. Wenzl [b], U. Scherf [c], C. Schmitt [c], R. Güntner [c], G. Leising [d]

[a] *Politecnico di Milano, Dip. di Elettronica e Informazione, Piazza Leonardo da Vinci 32, 20133 Milano, Italy*
[b] *Inst. für Festkörperphysik, Technische Universität Graz, Petersgasse 16, A-8010 Graz, Austria*
[c] *Polymerchemie, Inst. für Physikalische und Theoretische Chemie, Universität Potsdam, Karl-Liebknecht-Str. 24-25, D-14476 Golm, Germany*
[d] *Science and Technology, AT&S AG, Leoben, Austria*

Received 4 June 2001; received in revised form 10 November 2001; accepted 17 December 2001

Abstract

Noise spectroscopy is presented to be a powerful tool to investigate the current flowing in organic light emitting diodes (oLEDs) with high sensitivity. Measurements can be performed over the whole bias range of interest, from reverse bias up to high values of forward bias voltage. From these measurements one can gain insight into the microscopic conduction processes dominating the device current and obtain valuable information for improved device modeling. In particular it is shown that the low frequency power spectrum of the tested oLEDs has a power law dependence around $(1/f)^{1.3}$ almost irrespective of device characteristics and of measurement conditions. Additionally, noise spectra are also proposed as a means to sense the initial state and the growth of degradation phenomena in these devices. The onset of degradation is shown to be signaled by current spikes that reflect on a net increase of the white noise component of about three orders of magnitude in the power spectral density, when degradation is just hardly beginning to be visible as dark spots on the emitting surface. © 2002 Elsevier Science B.V. All rights reserved.

PACS: 72.80.Le; 73.50.Td; 85.60.Jb
Keywords: Degradation; Noise; Semiconducting polymer; oLED

1. Introduction

Light emitting diodes from organic materials, generally abbreviated as oLEDs, are the target of world wide research due to their possible application for low cost and easy processing full color large area displays [1]. For a further improvement of the performance of these diodes, a detailed knowledge of the charge injection and transport processes is of great importance. Such information is commonly gained by modeling current/voltage (I/V) and current/luminance (I/L) characteristics [2–6]. However, additional experimental methods to better disentangle the various physical phenomena (space charge limited current (SCLC), contact limited current, trapping, field dependent

* Corresponding author. Tel.: +39-02-2399-6188; fax: +39-02-2367-604.
E-mail address: marco.sampietro@elet.polimi.it (M. Sampietro).

1566-1199/02/$ - see front matter © 2002 Elsevier Science B.V. All rights reserved.
PII: S1566-1199(02)00023-X

charge carrier mobility, drift and diffusion currents) would be highly desirable. Furthermore, to fullfil the requirements necessary for commercial applications, a detailed investigation of the processes leading to device degradation is also necessary. Although there are a lot of studies known from the literature [7–12] concerning this topic, most of them are based on the observation of visible degradation of the diodes, that is after the degradation processes have summed up to visible damage of the devices. A method to study the degradation of the devices in earlier stages, this means at the very beginning of degradation, would therefore be of great importance. In the following, we will show that current noise spectroscopy is such a powerful tool that allows on one hand to study charge injection and transport phenomena and on the other hand it can be used to monitor the initial states of device degradation in oLEDs by a fast and easy computational scheme.

Noise measurements have been proved to be very important in the characterization of inorganic semiconductor materials or devices. The extensive literature covering this subject can be grouped into three main classes: (i) Noise measurements can be directly used to quantify the noise contribution of a new device when placed in a circuit to foresee the overall signal-to-noise ratio of the system [13]. (ii) Noise measurements can be indirectly used to investigate the statistical properties of the carrier transport and, for example, distinguish shot phenomena from trapping and detrapping, conductance fluctuations or contact injection [14]. (iii) Noise measurements can be indirectly used to measure other physical properties of the sample, such as device bandwidth, carriers transit time, carriers mobility and others [15].

Differently from inorganic semiconductor devices, noise investigations on organic devices are rare. Exceptions are a study on an oLED [16], some reports on organic transistors [17,18] and a report concerning current noise spectroscopy as a method to track conductance fluctuations in an oLED [19]. This low number of investigations of noise phenomena is astonishing, since the analysis of current fluctuations measured in oLEDs around mean value, as a function of both time and frequency, reveals the microscopic behavior of the organic devices and could give some additional information on the physics of carrier transport mechanisms. By varying the operating conditions of the devices, going from below-threshold to high voltage regimes in which electroluminescence occurs, all operating regimes can be easily explored.

The paper is structured as follows. Section 2 summarizes in a short overview the noise sources present in semiconductor devices together with their spectral distributions. Section 3 describes the Correlation Spectrum Analyzer that has been used to perform all noise measurements reported in this paper. Section 4 reports on the preparation and the properties of the organic devices used for the measurements. Section 5 comments the results from the noise measurements. Section 6 shows how noise can be used to sense the initial state and the growth of oLED degradation in large advance to other techniques. Finally some conclusions are drawn in Section 7.

2. Noise sources and spectral distributions

A device held at temperature T produces a minimum level of voltage or current fluctuation due to the random thermal motion of carriers. This noise, called Johnson noise, is characterized by a power spectral density constant with frequency (white), equal to $4kT/R$ [A^2/Hz] when measured as current fluctuations or $4kTR$ [V^2/Hz] when measured as voltage fluctuations, where R is the electrical resistance of the sample and k is the Boltzmann's constant (1.38×10^{-23} J/K) [20]. In a device held at thermodynamic equilibrium that is without any bias applied across its terminals or any other external perturbation like for example an incident photon flux the Johnson noise is the only noise present.

Whenever a device is brought out of thermal equilibrium, other noise contributions come into place. It is generally accepted that, if the carriers flowing across the device are emitted over a potential barrier, the random time distribution of the emission produces additional noise, called shot noise. It has a white power spectral density equal to $2qI$ [A^2/Hz], where I is the mean current flow-

ing through the sample and q is the electronic charge (1.602×10^{-19} C) [21].

In addition to the two mentioned fundamental noise sources, all devices out of equilibrium manifest additional "excess noise" that increases its power density as the frequency reduces. Because of this frequency behavior, this noise is also called, for simplicity, "$1/f$ noise". A very extensive literature is available investigating the sources of this excess noise in inorganic devices: it can be attributed to carrier conductance fluctuations [22,23], single carrier trapping and detrapping (also called "telegraphic noise") [24], defects and inhomogeneities of the crystal along the carriers path [25], and others. Each of these noise sources would give, if present alone, a spectrum with a defined power function of frequency of the type $A(1/f)^a$. In a real device many of these different microscopic noise sources are present and contribute to the final spectrum producing a power spectrum with $a \cong 1$. The dependence of both a and A as a function of bias and temperature can help to single out the actual noise sources. What is generally believed from the experience on inorganic semiconductors is that better crystal growing and cleaner production steps reduce the noise power amplitude A, and this consideration equally well applies to organic materials. In organic devices $1/f$ noise is largely dominating at frequencies below 1 MHz. Thermal noise, instead, is negligible under normal operating conditions.

3. Description of the noise measuring system

To perform Noise Spectral Analysis, the device is biased at the desired voltage and current fluctuations around its mean value are measured. A frequency analysis (Noise Spectroscopy) is carried out by computing the squared absolute value of the Fourier transform of the current fluctuations as a function of time, and by selecting the mean square value (power) of each frequency component of the signal (power spectrum) [26]. We have performed the noise analysis by using a Correlation Spectrum Analyzer [27].

The instrument, schematically shown in Fig. 1, is made of two separate and independent input amplifiers having transimpedance front-ends between which the device under test (DUT) is connected. This connection makes the instrument ideal for measuring directly the current noise produced by the DUT. Furthermore, the instrument is conceived to take full advantage of the correlation technique to measure the DUT noise irrespective of disturbances introduced by additional biasing components or by the instrument itself. In fact the oLED current noise is flowing through the two amplifiers and processed in parallel on the two channels, while the disturbances introduced by one amplifier are only present on its own channel. By performing a cross-correlation between the outputs of the two channels and averaging the results, the signal produced by the oLED is extracted and amplified while the residual disturbances are reduced proportionally to the square root of the measuring time. Therefore, very small oLED noise can be measured with high precision by simply extending measurement time.

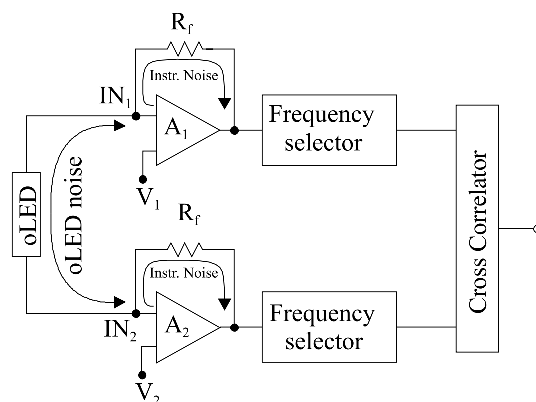

Fig. 1. Schematic of the Correlation Spectrum Analyzer used for noise measurements. The oLED device (DUT) is inserted between the two instrument input ports, IN_1 and IN_2, and biased at the desired voltage directly by the instrument through V_1 and V_2.

Another advantage of the Correlation Spectrum Analyzer is that the bias voltage across the DUT can be chosen at will and set directly by the instrument by trimmering the voltages V_1 and V_2 externally applied to each amplifier. Because of the high voltage gain of the differential amplifier A_1 (A_2), the external voltage V_1 (V_2) will be forced by the feedback resistor R_F to be applied to the node

IN_1 (IN_2) and therefore applied across the oLED sample. The measuring set-up consequently is greatly simplified and made more stable and precise. A detailed description of the instrument is given in [27]. The instrument operates on a frequency range from few mHz to almost 1 MHz and has a sensitivity down to 1 $fA/\sqrt{Hz}$.

4. Device samples and preparation

The polymer used for this study is a methyl substituted ladder type poly(para phenylene). Reports on blue and blue-green emitting oLEDs [28] and LECs [29,30], white light emitting oLEDs realized by an internal color conversion technique [31] and the application of mLPPP as an active material in solid state lasers [32], due to the fact that stimulated emission and photoinduced absorption do not compete [33], are only some examples of the outstanding properties of this kind of conjugated polymer.

To prepare the devices, mLPPP was dissolved in chloroform and stirred for one day at 60°C in argon atmosphere. ITO coated glass substrates were transferred after a wet cleaning process into an argon filled glove box and mLPPP was spin-coated on top of the substrates (using a 0.22 μm teflon filter), resulting in active layers extending from 80 nm (thin devices) to 160 nm thickness (by varying the concentration of mLPPP in chloroform). Afterwards, an aluminum top electrode with a thickness of about 200 nm was evaporated on the mLPPP layer to achieve active device areas of about 9 mm^2. To record the current noise spectra, the devices were mounted in a specially designed sample holder to investigate the devices in argon atmosphere.

5. Experimental results

In order to characterize the whole operation regime of the oLEDs, noise measurements were performed at different bias voltages: reverse bias, low forward bias (below the turn-on of the device), normal forward bias (slightly above the turn-on of the device) and high forward bias. The results presented in the following were obtained by exploring devices with thickness of 160 nm, except where otherwise mentioned.

The electrical characteristics of oLEDs prepared from mLPPP are well investigated [28]. Using ITO and Al as charge carrier injecting electrodes results in rather high turn on voltages since mLPPP is a wide band gap polymer with a rather high mismatch between its HOMO and LUMO and the work functions of the electrode materials. Additionally, as common for rigid rod polymers, the turn-on of the current is thickness dependent due to a preferential orientation of mLPPP chains close to the substrate surface: for thinner films a much higher field is necessary compared to thicker devices in which the turn on is characterized by the randomly distributed polymer chains in the bulk. From the reported [28] dependence of the electric field necessary for the onset of the current using ITO and aluminum as electrodes, a turn-on value of about 0.55 MV/cm is expected for mLPPP layers of 160 nm thickness, this means a voltage of about 9 V.

The devices to be tested were first biased in reverse direction (ITO wired as a cathode) in order to exclude influences of parasitic currents due to native microshorts in the active layer. The standing current was measured to be well below 100 nA in all selected devices up to a bias of −14 V, showing the good accomplishment of the above mentioned requirement and the high rectification ratio of mLPPP based oLEDs. As an example, Fig. 2 is the plot of the current as a function of

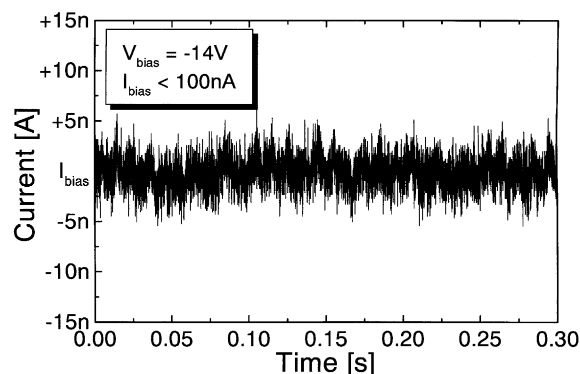

Fig. 2. Current noise versus time of an mLPPP based oLED with a reverse bias applied of 14 V.

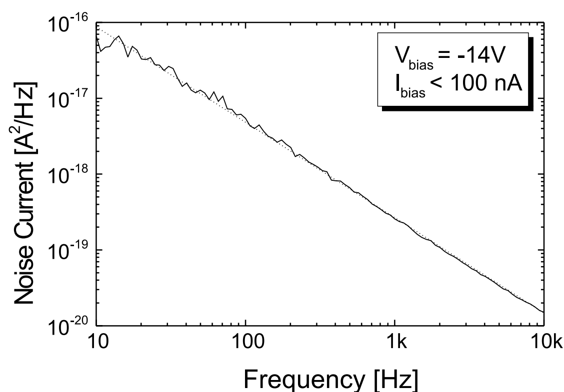

Fig. 3. Current noise versus frequency of an mLPPP based oLED with a reverse bias applied of 14 V.

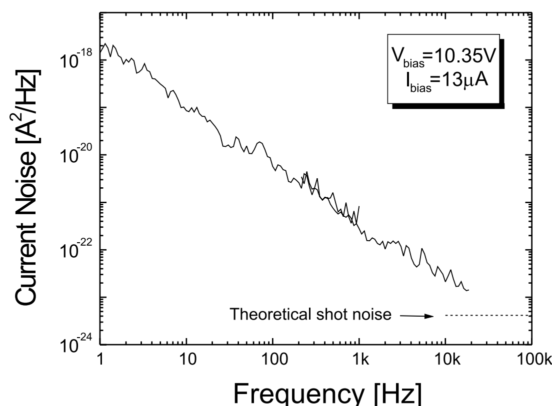

Fig. 4. Current noise versus frequency of an mLPPP based oLED with a forward bias applied of 10.35 V. The theoretical shot noise level is not reached within the possibilities of the measurement due to the large capacitance of the oLED.

time on one device and Fig. 3 is the corresponding noise spectrum. The current noise versus frequency shows that, within the measured frequency interval, the $(1/f)^a$ noise is largely dominant with respect to the thermal noise and to the shot noise (calculated using the equations mentioned in Section 2), this latter being at least five orders of magnitude below the measured excess $(1/f)^a$ noise. Note that the power spectrum is varying as $(1/f)^a$ with $a \cong 1.3$.

The noise spectra of the current flowing in the devices have then been measured for various bias conditions in forward mode, from low forward bias voltages to operating voltages above the threshold for electroluminescence. Fig. 4 reports, as an example, the current noise versus frequency plot for a device of 160 nm thickness biased slightly above the turn on voltage ($V_{\text{bias}} = 10.35$ V and $I_D = 13$ μA). The spectrum is again dominated by $(1/f)^a$ behavior and shows a slope of $a = 1.3$.

The analysis of the low frequency slope of all spectra taken reveals a significant constancy of its value through all biasing conditions. Regardless of the sign and value of the bias voltage, the slope of the $(1/f)^a$ plots remains between $a = 1.24$ and $a = 1.35$. The same behavior is also found for all the thinner devices investigated, as can be seen in the spectra given in Fig. 5. This signature in the slope of the noise spectra is evident and may be a guide in assigning this phenomenon also to other effects than trapping and detrapping from localized states deep in the gap of the material. Indeed, we note a striking similarity of these slopes with those found in inorganic devices at the earliest stages of their development and attributed to the microphysics of the contacts between the metal electrodes and the semiconductor in a fundamental work by Macfarlane [36] and called "contact noise". Contact noise theory applies to semiconductor devices with a nonhomogeneous adhesion of the two interfaces and assumes that the emission of carriers from the contacts takes place only at localized patches on the surface where adsorbed ions are present to give rise to a Schottky barrier

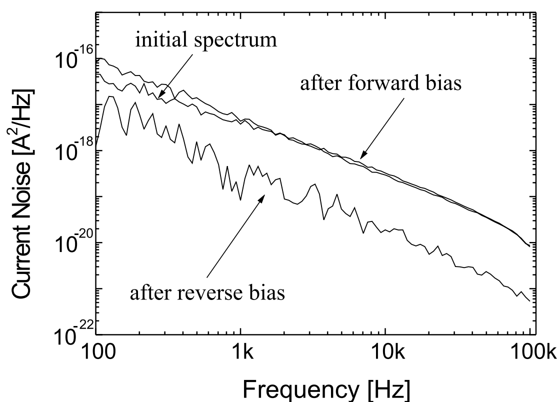

Fig. 5. Spectral noise measurements on a thin mLPPP oLED performed at the same bias condition, ($V_{\text{bias}} = 2$ V), after different bias sequences.

layer. Diffusion of the ions over the surface gives rise to random fluctuations of their concentration in a patch, which results in random fluctuations in the height of the potential barrier and therefore in the emitted current. The theory depicting this situation leads to $(1/f)^a$ spectra with a ranging from 1.1 to 1.5 depending on the frequency range of investigation and on the sample temperature. This phenomenon may apply to organic devices and finds support on the inhomogeneities of the ITO–mLPPP interface as well as of the Al–mLPPP interface, on contaminations due to the wet cleaning process of the ITO surface and on the inevitably poor adhesion between the active organic layer and the electrode materials, which makes the present situation of organic materials comparable to that of inorganic materials in former times. A systematic approach to test this phenomena is under way in our laboratory.

A behavior that has been noticed in our devices, also reported in previously published works [34,35], is the dependence on the bias history of the device. The noise level of the oLEDs under forward biasing conditions was found to strongly depend on whether the device was operated in reverse direction or in forward direction before performing noise measurements in the forward regime. Also in this type of investigations, spectral noise measurements may be a valid and sensitive tool to track this phenomenon, as in the example shown in Fig. 5. The figure specifically refers to a diode with thin organic layer, (80 nm), but similar behavior has been obtained also on all the other devices. A current spectrum was first measured in a given forward bias ($V_{bias} = 2$ V in the case of this example, corresponding to $I_D \cong 18$ μA), indicated with "initial spectrum" in the figure. Then the device had been biased over the threshold for several minutes, and then it was biased back to the initial bias value (again $V_{bias} = 2$ V and $I_D \cong 10$ μA). Spectrum was taken and indicated with "after forward bias" in the figure. This biasing treatment in forward direction had almost no influence on the current noise produced by the device in the low forward regime as evidenced in Fig. 5, where this two spectra nearly overlap. Afterward the device was biased in reverse bias ($V_{bias} = -4$ V) for some minutes after which it was biased back again to 2 V and spectrum taken. This latter is indicated with "after reverse bias" in the figure. In this latter case the noise produced by the device is much lower than measured initially at the same voltage. This noise reduction is only partly due to a corresponding reduction of the current flowing in the device, which slowly (transients of several minutes) tend to drift back to the value previously measured in the "initial" condition. The reverse bias effect on noise has a time duration which is instead much longer than current transients, indicating that a reassessment of transport phenomena is also taking place. Note that also in this experiment the measured power spectra vary as $(1/f)^a$, with a around 1.35; depending on the history of the device, the slope is little steeper after reverse bias. The white thermal and shot noise power spectrum are still negligible with respect to the excess noise in the tested frequency range.

6. Noise tracking of oLED degradation phenomena

Noise spectral analysis shows to be very effective also in tracking the initial state and the growth of catastrophic degradation in organic devices. We have tested this possibility in our oLEDs. In order to accelerate the degradation phenomena, the forward biasing of the same device used to record the above mentioned noise spectra has been increased from 10.35 V to a value of 16.25 V largely above the threshold. The device was carrying relatively high currents (about 485 μA, luminance 19 cd/m^2). Fig. 6 shows the time behavior of the current of the device on the way of its degradation. The degradation shows up as current spikes that can be directly seen in the current time plot and grow in rate by further increasing bias stressing. As discussed in [8,9], under high voltage stress very large currents always form prior to thermal breakdown and catastrophic failure. These spikes can therefore be assigned to the very initial states of such irreversible degradation.

Each of these spikes contributes to additional white noise and can be tracked with high sensitivity in the noise spectrum measurement. Fig. 7 shows the noise spectra produced by the current in this working condition. Indeed one can see (and

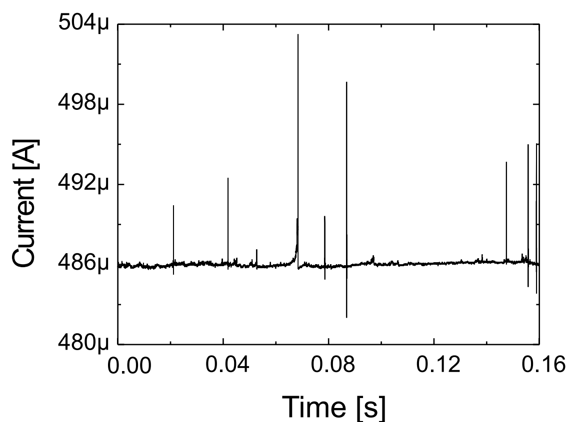

Fig. 6. Time plot of the current flowing in an oLED device at an overstressing bias of 16.25 V.

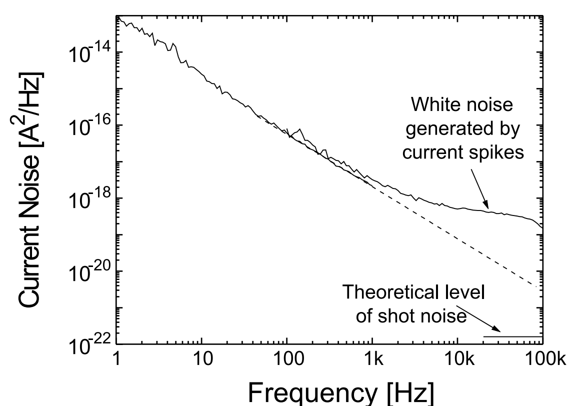

Fig. 7. Noise spectra of the current fluctuations in the device that is undergoing degradation (high forward bias). Also indicated in the figure (dotted line) is the fitting of the $(1/f)^a$ slope that the noise would attain in the case of absence of spikes ($a \cong 1.6$).

compare with Fig. 4, for example) that, besides an increase of noise in the low frequency part of the spectrum, at higher frequencies a flat noise spectral density is produced. The measured white noise level has increased by almost three orders of magnitude with respect to the theoretical value of shot noise ($\overline{i_n^2} = 1.6 \times 10^{-22}$ A^2/Hz) given by a standing current of $I_D = 485$ μA.

This high value of measured white noise precisely reflects the presence of the current spikes that are seen in Fig. 6. This can be easily proved as in the following. Let us assume, for simplicity, that each spike can be considered as a Dirac delta function of area equal to the carried charge Q_i. The global signal on a large time interval $2T$ can be considered as a repetition of spikes randomly distributed in time with a mean rate of occurrence equal to λ,

$$i(t) = \sum_{i=1}^{2\lambda T} Q_i \delta(t - t_i).$$

To calculate the power spectral density of this signal, we can conveniently compute its autocorrelation function,

$$R(\tau) = \langle i(t) i(t + \tau) \rangle,$$

where the symbol $\langle \cdot \rangle$ denotes time-averaging and we have assumed $i(t)$ ergodic. Thanks to the noncorrelation among the spikes, $R(\tau) = 0$ for every $\tau \neq 0$. At $\tau = 0$, instead, we obtain the mean square value of the current,

$$\langle i^2(t) \rangle = \lim_{T\to\infty} \frac{1}{2T} \int_{-T}^{T} \sum_{i=1}^{2\lambda T} Q_i^2 \delta(t - t_i)\, \mathrm{d}t$$
$$= \lim_{T\to\infty} \frac{1}{2T} \sum_{i=1}^{2\lambda T} Q_i^2 = \lambda \overline{Q^2},$$

where $\overline{Q^2}$ is the mean square value of the spike charge. The autocorrelation function is therefore

$$R(\tau) = \lambda \overline{Q^2} \delta(\tau).$$

The corresponding bilateral power spectral density is the Fourier transform of $R(\tau)$, so

$$S_i(f) = \mathrm{FT}[R(\tau)] = \lambda \overline{Q^2},$$

that shows to be frequency independent (white) and proportional to the rate of spikes [26]. By taking the mean number of spikes from the experimental situation given in Fig. 6 as being about $\lambda = 50$ spikes/s, their mean amplitude of about 9 μA and their mean time base equal to 5 μs (see Fig. 8 for an expanded view of one spike), we finally obtain $\overline{Q^2} \cong 2 \times 10^{-21}$ C^2 and a physical (unilateral) spectral density of $2\lambda\overline{Q^2} \cong 2 \times 10^{-19}$ A^2/Hz, which well agrees with the level of the measured white spectrum indicated in Fig. 7.

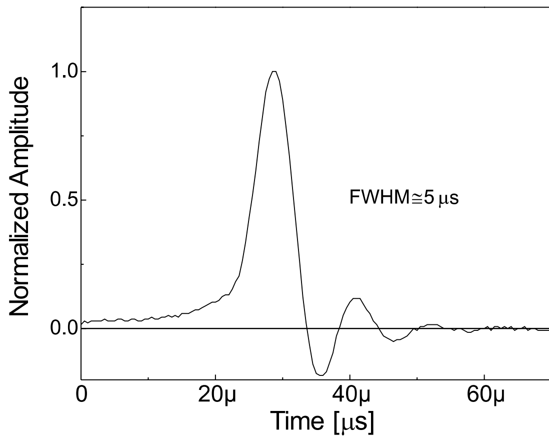

Fig. 8. Detail of one spike on an expanded temporal axis.

By keeping the device in the biasing condition in which spikes are present, the number of spikes per second does not change significantly while the average current carried by the device continuously decreases. Fig. 9 shows the reduction in the average current on a percentage scale as a function of time from the moment the spikes have started to appear. The time scale of the figure is of several minutes while the time interval between spikes is of few hundredths of second. At the end the device undergoes a catastrophic failure with macroscopic evidences of degradation in the form of visible dark spots and enhanced cathode surface roughness. These effects of spotty metal evaporation and delamination, in addition to possible localized polymer degradation, by reducing the effective device area are the reasons of the current reduction on a long time scale.

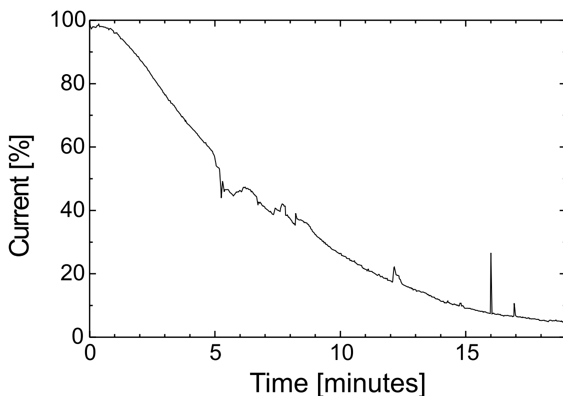

Fig. 9. Evolution with time of the average current carried by an oLED undergoing degradation.

The observation of the additional white noise component superimposed on the current noise spectra of oLEDs on the way of degradation may be efficiently used to detect the onset of device degradation. Thanks to the proportionality of the white noise spectral density to the mean rate of occurrence of the spikes and to the charge carried by each spike, the time evolution of the degradation can be almost on-line monitored by restricting the evaluation of the spectral density to a limited frequency range in the flat region, for example around 100 kHz in our case, to be extremely fast in computation. Fig. 10 shows the sensitivity that one might obtain with such a measurement in terms of the excess measured white noise generated by current spikes with respect to the theoretical level of shot noise, ($\overline{i_n^2} = 1.6 \times 10^{-22}$ A^2/Hz, upper curve), or with respect to the pre-degradation value of $1/f$ noise that would be measured if the spikes were not present (taken as $\overline{i_n^2} = 3 \times 10^{-21}$ A^2/Hz, see dotted line in Fig. 7 at 100 kHz). The sensitivity of the noise measurement would be such

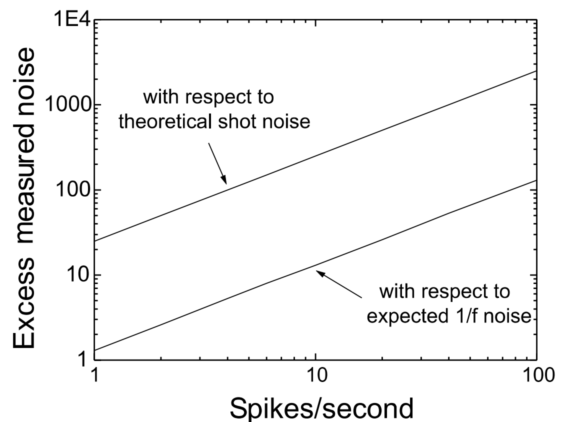

Fig. 10. Excess measured white noise generated by current spikes as a function of the number of spikes per second, λ. The upper curve refers to the ratio between the excess measured noise and the theoretical level of shot noise ($\overline{i_n^2} = 1.6 \times 10^{-22}$ A^2/Hz) given by a standing current of $I_D = 485$ μA. The lower curve refers to the ratio between the excess measured noise and the expected $1/f$ noise ($\overline{i_n^2} = 3 \times 10^{-21}$ A^2/Hz, see dotted line in Fig. 6 at 100 kHz) that would be measured if the spikes were not present.

that few spike/s would give a noise spectral density at least one order of magnitude higher than the pre-degradation value. The spectral measurement therefore confirms as a very powerful tool to gain information related to the very initial degradation process. When a deviation from the pre-degradation value of $1/f$ noise occurs, device operation can be stopped and all necessary structural or spectroscopic analysis can be performed on the device to investigate the sources that give reason of degradation, before the microscopic damages sum up to a visible and irreversible macroscopic failure.

7. Conclusions

We have shown that noise spectroscopy is a powerful spectroscopic method to investigate the different operation regimes, (from reverse direction up to high forward biases), of organic light emitting diodes and can therefore give valuable information to improve device modeling. The devices tested in this studies had a simple single layer set up with a methyl substituted ladder type poly(para phenylene) embedded between an ITO and an Al electrode. From reverse bias up to biases slightly above the turn-on of the devices the current noise curves have similar slopes. From this behavior and the corresponding value of the slope, it can be inferred that the metal electrode/organic layer interfaces are dominating the current noise plots. One should note that the devices here were prepared by a simple wet pre-cleaning process of the substrates; further improvements of the pretreatment of the substrates and of the metal electrode/ organic layer interfaces may result in a current noise no more dominated by contact phenomena but by intrinsic transport properties of the organic bulk. Additionally, information gained by current noise spectroscopy is also very promising for a further improvement of device lifetimes, since degradation of the devices was found to give reason for a white power spectrum superimposed on the slope of the pre-degradation current noise plot. This behavior can be applied to detect the early beginning of degradation of the devices under operation with high sensitivity by a fast and easy computational scheme; in combination with other spectroscopic methods conclusions could be drawn on the processes resulting in the irreversible macroscopic failure of the devices.

Acknowledgements

The financial support by Italian MURST and CNR and Austrian FWF project P14170-TPH are gratefully acknowledged.

References

[1] R.H. Friend, R.W. Gymer, A.B. Holmes, J.H. Burroughes, R.N. Marks, C. Taliani, D.D.C. Bradley, D.A. Dos Santos, J.L. Bredas, M. Lögdlund, W.R. Salaneck, Nature 397 (1999) 121.

[2] P.S. Davids, I.H. Campbell, D.L. Smith, J. Appl. Phys. 82 (1997) 6319.

[3] J. Staudigel, M. Stößel, F. Steuber, J. Simmerer, J. Appl. Phys. 86 (1999) 3895.

[4] B.K. Crone, I.H. Campbell, P.S. Davids, D.L. Smith, C.J. Neef, J.P. Ferraris, J. Appl. Phys. 86 (1999) 5767.

[5] V.I. Arkhipov, E.V. Emelianova, Y.H. Tak, H. Bässler, J. Appl. Phys. 84 (1998) 848.

[6] P.W.M. Blom, M.C.J.M. Vissenberg, J.N. Huiberts, H.C.F. Martens, H.F.M. Schoo, Appl. Phys. Lett. 77 (2000) 2057.

[7] J.C. Scott, J.H. Kaufman, P.J. Brok, R. DiPietro, J. Salem, J.A. Goitia, J. Appl. Phys. 79 (1996) 2745.

[8] L.S. Liao, J. He, X. Zhou, M. Lu, Z.H. Xiong, Z.B. Deng, X.Y. Hou, S.T. Lee, J. Appl. Phys. 88 (2000) 2386.

[9] X. Zhou, J. He, L.S. Liao, M. Lu, X.M. Ding, X.Y. Hou, X.M. Zhang, X.Q. He, S.T. Lee, Adv. Mater. 12 (2000) 265.

[10] J. McElvain, H. Antoniadis, M.R. Hueschen, J.N. Miller, D.M. Roitman, J.R. Sheats, R.L. Moon, J. Appl. Phys. 80 (1996) 6002.

[11] V.N. Savvateev, A.V. Yakimov, D. Davidov, R. Pogreb, M.R. Neuman, Y. Avny, Appl. Phys. Lett. 71 (1997) 3344.

[12] S.T. Lee, Z.Q. Gao, L.S. Hung, Appl. Phys. Lett. 75 (1999) 1404.

[13] A. van der Ziel, Noise in Measurements, John Wiley & Sons, New York, 1976.

[14] See various papers in Proceedings of the 15th International Conference on Noise in Physical System and $1/f$ Noise, Bentham Press, London, 1999.

[15] M. Sampietro, G. Ferrari, G. Bertuccio, J. Appl. Phys. 87 (2000) 7853.

[16] P. Herve, Thesis, Eindhoven University of Technology, 1997.

[17] P.V. Necliudov, S.L. Rumyantsev, M.S. Shur, D.J. Gundlach, T.N. Jackson, J. Appl. Phys. 88 (2000) 5395.

[18] S. Martin, A. Dodabalapur, Z. Bao, B. Crone, H.E. Katz, W. Li, A. Passner, J.A. Rogers, J. Appl. Phys. 87 (2000) 3381.
[19] M. Sampietro, G. Ferrari, D. Natali, U. Sherf, K.O. Annan, F.P. Wenzl, G. Leising, Appl. Phys. Lett. 78 (2001) 3262.
[20] J.B. Johnson, Phys. Rev. 32 (1928) 97.
[21] W. Schottky, Ann. Phys. 57 (1918) 541–567.
[22] L.K.J. Vandamme, IEEE Trans. Electron Devices 41 (1994) 2176.
[23] A. van der Ziel, IEEE Proc. 76 (1988) 233.
[24] K. Kandiah, M.O. Deighton, F.B. Whiting, J. Appl. Phys. 66 (1989) 937.
[25] F.N. Hooge, IEEE Trans. Electron Devices 41 (1994) 1926.
[26] J.S. Bendat, Principles and Applications of Random Noise Theory, John Wiley & Sons, New York, 1958.
[27] M. Sampietro, L. Fasoli, G. Ferrari, Rev. Sci. Instrum. 70 (1999) 2520.
[28] S. Tasch, A. Niko, G. Leising, U. Scherf, Appl. Phys. Lett. 68 (1996) 1090.
[29] S. Tasch, J. Gao, F.P. Wenzl, L. Holzer, U. Scherf, K. Müllen, A.J. Heeger, G. Leising, Electrochem. Solid State Lett. 2 (1999) 303.
[30] M. Sampietro, R. Sotgiu, F.P. Wenzl, L. Holzer, S. Tasch, G. Leising, Phys. Rev. B 61 (2000) 266.
[31] S. Tasch, E.J.W. List, O. Ekström, W. Graupner, G. Leising, P. Schlichting, U. Rohr, Y. Geerts, U. Scherf, K. Müllen, Appl. Phys. Lett. 71 (1997) 2883.
[32] G. Kranzelbinder, G. Leising, Rep. Prog. Phys. 63 (2000) 729.
[33] W. Graupner, G. Leising, G. Lanzani, M. Nisoli, S. De Silvestri, U. Scherf, Phys. Rev. Lett. 76 (1996) 847.
[34] W. Brütting, H. Riel, T. Beierlein, W. Riess, J. Appl. Phys. 89 (2001) 1704.
[35] W. Brütting, S. Berleb, A.G. Mückl, Org. Electr. 2 (2001) 1.
[36] G.G. Macfarlane, Proc. Phys. Soc. B LXIII (1950) 807.